JOURNAL OF THEORETICAL AND APPLIED MECHANICS
48, 4, pp. 957-972, Warsaw 2010

DYNAMIC FRAGMENTATION OF LASER SHOCK-MELTED METALS: SOME EXPERIMENTAL ADVANCES

Thibaut De Resseguier, Didier Loison, Emilien Lescoute, Loic Signor, Andre Dragon

Institut Pprime, CNRS–ENSMA–Université de Poitiers, Département Physique et Mécanique des Matériaux – ENSMA, Futuroscope – Chasseneuil Cedex, France
e-mail: resseguier@ensma.fr; didier.loison@ensma.fr; andre.dragon@ensma.fr

While spall damage in solid materials has been one of the most widely studied shock-driven phenomena, very little data can be found yet about spallation in liquid metals. In recent papers, some of present authors have reported on exploratory investigations of liquid spall – sometimes called "microspall" – in tin samples melted upon laser shocks of high intensities. Modelling approaches have also been discussed and compared with experimental observations. In particular, theoretical fragment size distributions have been compared with experimental distributions inferred from image analyses on fragment-impacted recovery polymer shields. While the curves representing the number per unit area vs. size of fragments present a similar aspect, the numbers predicted by an energy-based model are significantly greater than those observed experimentally. This is due predominantly to the characterisation technique, limited to surface examination, while a number of fragments penetrate the polymer shield and lay below its surface. This is why a new fragment recovery technique is being tested in this paper. This technique, based on a highly transparent low density gel, allows soft recovery and easier observation (compared e.g. with foams or aerogels) of the fragments size, shape and penetration depth, with improved spatial resolution. Coupled with shadowgraphy, scanning electron micrography and optical micrography, this recovery technique progress allows for an advanced insight into the phenomenology of microspall related fragmentation. To show it, laser shocks upon a tin target and an aluminium target are investigated, leading to different scenarios regarding melting conditions and fragmentation processes.

Key words: laser shock, fragmentation, liquid spall, shadowgraphy, fragment recovery, tin, aluminium

1. Introduction

The development of high energy laser facilities dedicated, for example, to inertial confinement fusion, has prompted the question of debris ejection from metallic shells subjected to intense laser irradiation (and consecutive mechanical shock effects) as an even more important issue for both fundamental and applied research. Whereas spall fracture in solid materials has been extensively studied for many years, see for example the synthesis by Antoun *et al.* (2002), scarce data can be found yet about fragmentation occurring after partial or full melting upon shock compression or release. In this context, we have set off a research programme based on laser driven shocks on tin targets, tin being chosen as a reference metal due to its low melting curve in the pressure-temperature diagram. The dynamic fragmentation ranging from the microspall process (ejection of a cloud of fine droplets) occurring upon reflection of the compressive pulse from the target free surface to the late rupture observed in the unspalled melted layer (leading to formation of larger fragments) has been in the centre of interest. These experiments provided some insight into the fragmentation process by combining time-resolved velocity measurements with post-shock observations of the recovered targets and fragments collected on polycarbonate (PC) shields (de Resseguier *et al.*, 2007a) or in low density foams (Signor *et al.*, 2007). Transverse visualization of the fragments ejection has been further developed (de Resseguier *et al.*, 2008). At the same time, some modelling issues have been addressed (Signor *et al.*, 2008, 2010). In the second paper cited, an energy-based fragmentation model inspired by Grady (1988, 1996) was introduced in the form of a cumulative failure criterion in a one-dimensional hydrocode allowing for comparisons between theoretical predictions and experimental observations. Further analyses, both experimental and interpretative, in relation to the aforementioned model, are given in de Resseguier *et al.* (2010). Figure 1, coming from this paper, shows fragment size distributions after a 140 GPa laser shock applied onto a 50 μm-thick tin target. The dotted line traces results from a numerical simulation employing the energetic criterion of Grady corresponding to the above laser shock. The experimental distributions inferred from the image analysis on the fragment-impacted surface of the PC shield match fairly with the aspect of the theoretical curve thus indicating a sort of qualitative consistency between the experiment and theory. However, fragment numbers per unit area predicted by numerical simulations are significantly greater than those observed experimentally. The major cause of this discrepancy is the penetration of a large percentage of tin fragments into the PC shield, i.e., below its surface.

It is confirmed by side views through the transparent shields reported in de Resseguier *et al.* (2010) and earlier in de Resseguier *et al.* (2007a). Smaller fragments should be ejected at higher velocities and undergo less drag during penetration than larger ones. They should imbed more easily into PC, while larger fragments are found on the shield surface. This is consistent with the data of Fig. 1, where the discrepancy between theoretical and observed fragment numbers decreases with increasing fragment size.

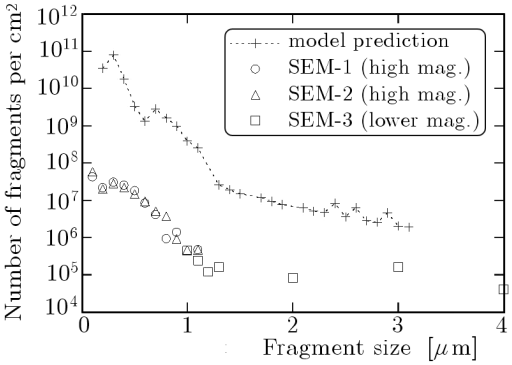

Fig. 1. Fragment size distributions after a 140 GPa laser shock applied onto a 50 μm-thick tin sample. The *dotted line* results from a one-dimensional simulation of the experiment using a global energetic criterion to account for the micro-spall process. The circles and triangles show experimental values provided by image analysis of Scanning Electron Micrographs (SEM) at high magnification. The very good match between two different pictures (both in the central zone of the impacted surface) seems to indicate that the results do not depend much on the choice of the observed area. The squares are obtained from a lower magnification SEM view, where larger fragments can be observed but sub-μm particles cannot be properly detected (coming from de Resseguier *et al.*, 2010)

This is the reason for searching more effective recovery techniques making possible a better quantification of the fragments size and number including particles which penetrate the shield. In this way, soft recovery of the ejecta is performed in this work within a low density gel where the fragments can be observed by post-shot optical microscopy with a resolution of μm-order. Such a post-shock analysis is coupled with other diagnostics to investigate fragmentation processes like microspalling and microjetting (this term designates three-dimensional effects governed mainly by target surface roughness leading to the ejection of thin 'jets' at very high speed). Currently, the most common diagnostic to study dynamic fragmentation is the VISAR-interferometer (Barker and Hollenbach, 1972) which allows time-resolved measurements of the target free-surface velocity. However, it is based on the probe light reflected

from this surface while the reflectivity at stake is lost when the aforementioned processes produce a cloud of micrometric debris. The transverse shadowgraphy is an alternative technique giving quasi-instantaneous pictures of ejected fragments at controlled delay times after the laser shot. Mean ejection velocities can be estimated from such pictures but low spatial resolution and integration across the transverse direction limit the characterisation of the fragments population. To discriminate within a field of velocities, as e.g. for a cloud composed of particles with different velocities, the Heterodyne Velocimetry (HV) technique has been recently developed and seems promising. It has been successfully applied to laser shock induced fragmentation (Mercier *et al.*, 2009). These comments put stress on the complementarity of the methods employed. Here, shadowgraphy and optical micrography images are being exploited in order to work out a more precise phenomenology of (i) reference microspall produced in a thin tin sample and (ii) spallation in a partially melted aluminium target. In both cases, the ejected fragments are recovered in a low density gel. The shock pressure decay in the aluminium target is computed in order to explain the fragmentation scenario different from the reference case (i).

The microspall phenomenology and the experimental setup employed are summarized in Section 2. The main observations regarding the test (i) are briefly given in Section 3, with a focus on the use of the new recovery technique. A more extensive analysis of the test (ii) is proposed in Section 4. The corresponding interpretations of fragmentation processes are presented in Section 5. Concluding remarks (Section 6) and references end the paper.

2. Microspall phenomenology and experimental setup

When a high power pulsed laser beam is focused onto the surface of an opaque sample, a thin layer of material is vaporised into a plasma cloud. The expansion of this plasma cloud towards the laser source drives by reaction a compressive pulse into the solid sample (target), see Figs. 8a and 9a. This is an essential feature regarding laser-matter interaction summarizing the transformation of laser irradiation into pressure pulse. The resulting strain rates are about 10^7 to $10^8\,\mathrm{s}^{-1}$, higher than those commonly attained under explosive loading or in plate impact experiments. If the diameter of the irradiated spot is much greater than the sample thickness and if the laser energy distribution is spatially uniform, the assumption of a planar wave front with conditions of uniaxial strain in the target region around the laser axis is a good approximation. During propagation through the sample, the compression wave gets steeper and

the release wave spreads, so the pressure profile becomes essentially triangular, and the peak pressure decays. As far as the amplitude of this pressure load is beyond the melting pressure (about 60 GPa for tin), the material is melted on compression. For lower amplitudes (between 20 and 60 GPa for tin), it can be melted fully or partially on release from the compressed state (Elias *et al.*, 1988; Eliezer *et al.*, 1990).

Upon shock breakout at the free surface of the target, three-dimensional effects governed predominantly by surface roughness can lead to ejection of thin jets at very high speed, usually termed as microjetting (Asay *et al.*, 1976). Employing targets with smooth surfaces, as in our previous experiments (the order of magnitude for roughness of $\sim \mu$m), this process is usually limited to extremely small masses, see Fig. 8b.

The seminal monograph by Nowacki (1978) gives detailed insights into wave propagation issues; the propagation of plane shock waves is dealt with in Chapter III of this book.

The reflection of the shock from the free surface produces a release front, and the interaction of this reflected wave with the incident unloading wave gives rise to tensile stresses over a layer of finite thickness beyond the free surface. For the solid material, this interaction of the two release waves can lead to the well-known spallation fracture by nucleation, growth and coalescence of voids or microcracks. If the material has been melted on compression or on release, the interaction occurs in a liquid state, which cannot bear intense tension. Instead of the aforementioned spallation (solid state), a microspall (or liquid spall) takes place (Andriot *et al.*, 1984), leading to material fragmentation into fine droplets ejected from the whole layer subjected to tensile loading. In Fig.8c, concerning a thin tin sample (50 μm) subjected to high loading pressure, this layer matches the sample thickness, so the whole target is fragmented into a microspall. This is not the case in general for thicker targets and moderate pressure (see de Resseguier *et al.*, 2010). The unspalled molten layer may separate into large liquid secondary fragments, turning into spherical drops under the action of surface tension.

In the experiments reported here, two complementary techniques have been used to investigate shock-induced dynamic fragmentation. First, optical transverse shadowgraphy provides successive pictures of the debris ejected from the sample, using a continuous laser probe to light up the gap behind the target and the afocal system (Fig. 2). The beam is divided with a pellicle beamsplitter and sent to two cameras with controlled delay times and an acquisition duration of 10 ns, which ensures minimum motion blur (typically 10 μm for a particle ejected at 1 km/s). Mean ejection velocities can be estimated from

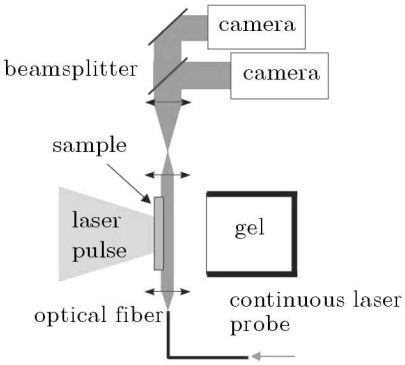

Fig. 2. Schematic of the experimental setup. Fragments ejected from the laser shock-loaded sample are observed by transverse shadowgraphy then collected in a transparent gel (Lescoute *et al.*, 2009)

such pictures, but low spatial resolution, speckle background due to the coherent laser probe light, and integration across the transverse direction strongly limit the characterisation of the fragments population. Therefore, soft recovery of the ejecta has been performed to complement the results. In previous tests, such recovery has been achieved in foams (see Signor *et al.*, 2010), but their analysis requires X-ray radiography and/or tomography. Here, a gel composed of hydrocarbon and polymer is set about 1 to 2 cm behind the sample free surface (Fig. 2). Its low density of $0.9\,\mathrm{g/cm^3}$ favours soft collection of the debris, while its high transparency allows easy observations of the recovered fragments with a μm-order resolution. Both the gel and the sample are placed in a vacuum chamber (10^{-4} mbar) to avoid laser breakdown in air before reaching the sample surface.

3. Soft recovery of microspalled ejecta from a tin sample

In this short section, some exploratory results are given as a reference illustration regarding the application of the new recovery technique based on the low density gel. The target is a 50 μm-thick tin sample of 99.99% purity. The experiment was performed in the *Laboratoire pour l'Utilisation des Lasers Intenses* (LULI, UMR CNRS 7605, Ecole Polytechnique, France). A laser pulse of 1.06 μm wavelength, 4 ns duration and 868 J energy was focused onto a 2 mm diameter spot in the target surface, leading to a $6.9\,\mathrm{TW/cm^2}$ intensity. The corresponding laser-matter interaction computation indicates a $\sim$ 135 GPa

peak loading pressure applied on the irradiated surface. Thus, the test is very similar to that reported above (Fig. 1, de Resseguier *et al.*, 2010), but the ejecta are collected here in a gel set 2 cm away from the target free surface instead of a PC shield.

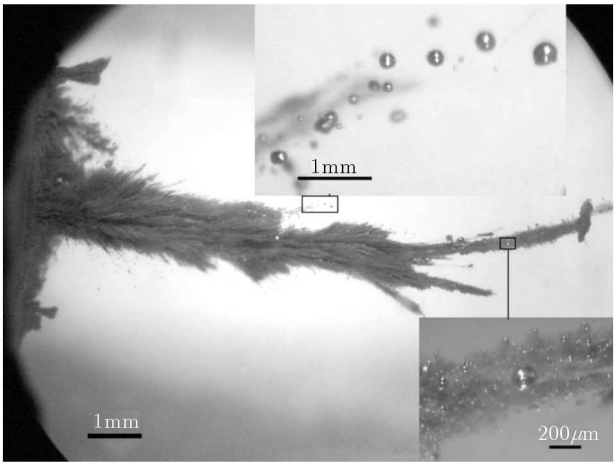

Fig. 3. Optical micrographs of fragments recovered in a gel set behind a 50 μm-thick tin target subjected to a 4 ns laser shot at 6.9 TW/cm^2. The impact surface in the gel is vertical, with debris penetrating from left to right

Figure 3 shows optical micrographs through the gel recovered after the experiment. Fragments penetrated up to 10 mm over a zone of 2-3 mm diameter in the transversal direction. Most fragments are approximately spherical which indicates that they result from the fragmentation process in the liquid state, so confirming full microspalling expected in this shot. The observations strongly suggest that most ejected particles are present in the gel, and that their shape and size have not been deeply affected by their impact and penetration. Thus, this new technique for fragment collection appears softer than the former PC shields, where large uncertainties had arisen from possible effects such as secondary fragmentation upon impact or rebounds from the shield surface. Although few solidified droplets of $\sim 100\,\mu$m diameter can be seen, the wide majority of observed fragments have a size of about $10\,\mu$m and less. This is fully consistent with previous results concerning tin debris collected in PVC foam for similar shock conditions, as shown in Signor *et al.* (2010). Smaller fragments are not resolved due to the limitations of optical microscopy employed here. Actually, the stream-like wakes of dark-grey traces are filled with sub-μm tin droplets. To enter into these wakes and characterise such small embedded debris, high-resolution (up to 0.3 μm) X-ray micro-tomography has

been planned. Furthermore, calibration work is needed to be able to correlate the impact velocity of a particle of known size and mass with its penetration depth in the gel, so that ballistic properties of the fragments within the microspall can be estimated.

4. Dynamic fragmentation of aluminium in the vicinity of melting point

Controlling spallation processes – including liquid spalling in the full meaning of the term 'spallation' here – is crucial in many fields where structural materials are subjected to intense shock loading, such as pyrotechnics, armor design, or inertial confinement fusion, for which the question of debris ejection from metallic shells submitted to intense laser irradiation has become a key issue in order to anticipate and reduce damage to optics and other equipment impacted by ejecta. This is why research programmes on spallation concern a large class of engineering materials. As regards our specific programme on dynamic fragmentation of metals below and above melting, it is evident that starting from tin, considered as a reference material, further research effort is to be made for more commonly applied structural metals. In this section, some exploratory results are given for aluminium using the setup described in Section 2.

The target is a 200 μm-thick aluminium foil. The experiment was performed in the Centre d'Etudes Scientifiques et Techniques d'Aquitaine (CESTA, CEA, Le Barp, France), on the Alisé laser facility. A laser pulse of 1.06 μm wavelength, about 3 ns duration and 157 J energy was focused onto a 1.7 mm spot, leading to a 2.6 TW/cm^2 intensity and an 80 GPa peak loading pressure on the sample surface, according to laser-matter interaction computations with the code CHIC of the *Centre Lasers Intenses et Applications* (CELIA, UMR CNRS 5107, France). Information regarding the fragmentation process is provided by means of (i) scanning electron micrographs of the rear (free) surface of recovered target (Fig. 4), (ii) optical micrographs of fragments recovered in the gel described above (Fig. 5), (iii) optical transverse shadowgraphs of the fragments ejected from the sample free surface; one shadowgraph is shown in Fig. 6. The central part of the target has been removed, the edges of the hole show clear evidence of resolidification after melting, and the ring between this melted edge and the outer unaffected zone presents a rough fracture surface typical of ductile fracture (Fig. 4). Such features, very similar to previous observations in tin samples (see de Resseguier *et al.*, 2007b, 2010),

might suggest microspalling. However, the ejecta collected in the gel (Fig. 5) are clearly different from those recovered from the tin target (see Section 3 and Fig. 3). Indeed, a large (∼mm size), single, roughly penny-shaped fragment has penetrated about 7 mm deep into the gel. Large amounts of much smaller debris are found mostly behind that main fragment. While most of these debris have irregular shapes, some spherical particles, indicative of fragmentation in liquid state, are detected (see detailed views in Fig. 5). The shadowgraph in Fig. 6 has been recorded 1 μs after the laser shot. It shows the expansion of a debris cloud from the free surface. Despite the speckle background due to transverse illumination by a laser source, such images provide a good estimate of the mean ejection velocity of the fastest fragments, about 3500 m/s in this experiment.

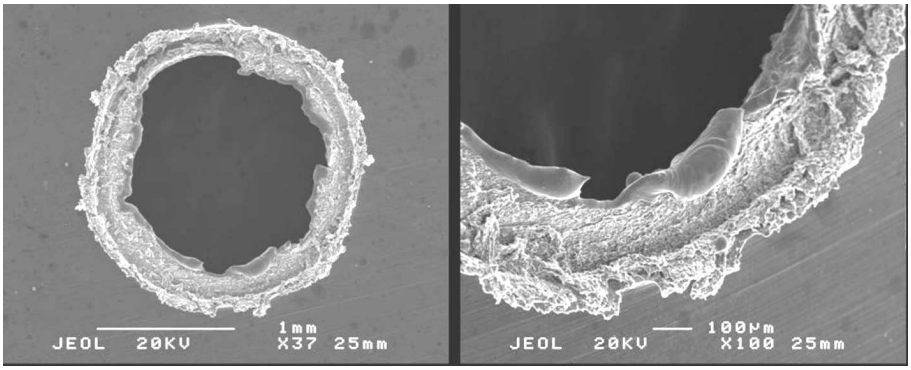

Fig. 4. Scanning electron micrographs of the free surface of a 200 μm-thick aluminium target after a 2.6 TW/cm^2 laser shot

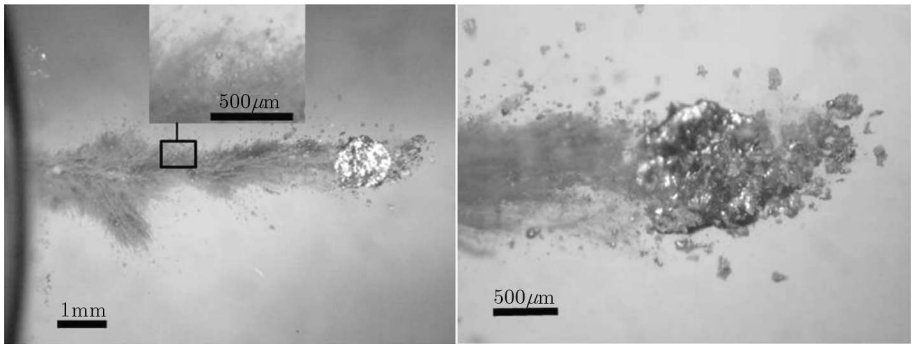

Fig. 5. Optical micrographs of fragments recovered in a gel set behind a 200 μm-thick aluminium target subjected to a 2.6 TW/cm^2 laser shot. The impact surface in the gel is vertical, with debris penetrating from left to right

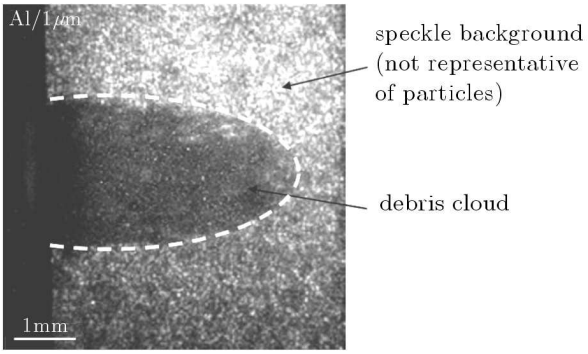

Fig. 6. Shadowgraph behind a 200 μm-thick aluminium sample 1 μs after a 2.6 TW/cm^2 laser shock applied onto the left surface (not shown). A debris cloud (delimitated by the white line for clarity) is ejected from left to right, with a peak ejection velocity of about 3500 m/s

To interpret the experimental data reported above, 1D computations of shock wave propagation using the code CHIC with a tabulated BLF equation of state (Bushmann *et al.*, 1992) for aluminium have been performed to estimate the peak pressure values throughout the sample thickness, notably near the spalled regions, taking into account the decay of the pressure pulse during its propagation from the loaded surface (Fig. 7). It can be seen that shock pressure decays from ~ 80 GPa near the irradiated surface to ~ 33 GPa beneath the free surface. From the pressure-temperature-phase diagram and Hugoniot curve of aluminium (Henis and Eliezer, 1993) one can infer that this metal would fully or partially melt on release from shocked states between about 60 GPa and 100 GPa (where the Hugoniot would meet the melting curve). Hence, a ~ 65 μm-thick layer beneath the irradiated surface of the laser shock-loaded sample would be partially melted, but the reflection of the compressive pulse from the free surface would take place in solid aluminium, where the interaction of the incident and reflected release waves would induce tensile stresses of increasing intensity, until reaching the so-called 'spall strength' of the material. This value, considered as the threshold tensile stress for damage initiation, is known to strongly depend on the strain rate (see Antoun *et al.*, 2002; Klepaczko and Chevrier, 2003). Under laser shock loading conditions, it has been reported to be about 1.6 GPa for solid aluminium (Tollier and Fabbro, 1998). Considering the shorter duration of the laser pulse leading to a higher strain rate in the present experiment, it has been set to 1.8 GPa in the simulation. According to that simulation, several spalled layers would separate successively from the free surface. The first, fastest one would be ejected at 3300 m/s. This prediction is in fair agreement with the maximum velocity of about 3500 m/s inferred from the shadowgraph (Fig. 6).

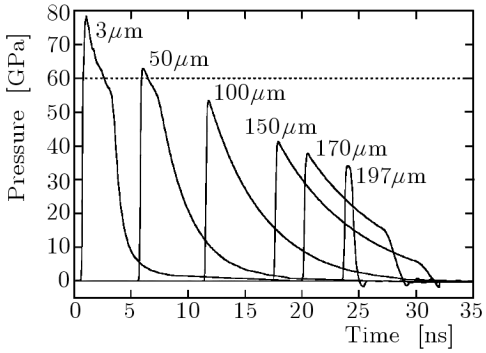

Fig. 7. Pressure profiles computed in a 200 μm-thick aluminium sample subjected to a 2.6 TW/cm^2 laser shock, at increasing distance from the loaded surface (from 3 μm t0 197 μm). The dotted line represents the 60 GPa threshold pressure for partial melting on release

5. Discussion

As pointed out earlier, high power pulsed laser irradiation produces the ablation of a thin layer (micrometer thick) of target material. The expansion of this layer, transformed into a plasma cloud, induces by reaction a compressive pulse onto the solid target (duration of $\sim$ 3-4 ns for the two experiments considered). The loading pressure pulse is imposed as a mechanical boundary condition on the irradiated target surface. During its propagation through the target, the compression front gets steeper, turning into a shock front and the unloading wave spreads. The pressure profile becomes roughly triangular (sometimes called unsupported shock wave or Taylor like wave) and the peak pressure decays. The reflection of this triangular compressive pulse from the opposite free surface of the target generates tension whose intensity should increase with distance from that surface. The dynamic fragmentation of the target sample may involve the following processes: (i) microjetting, (ii) spall fracture, (iii) microspallation after melting, depending on the loading conditions, target thickness and surface roughness. Both shots analysed in this paper by complementary techniques involve some melting, respectively in tin and aluminium, but they present highly contrasted scenarios.

The 50 μm-thick tin foil subjected to a 135 GPa laser shock is fully melted, predominantly on compression, then completely microspalled over its whole thickness. The corresponding gel is free from large fragment, fine droplets are recovered with a wide range of penetration depths indicative of a wide range of ejection velocities, mostly in the axial direction, and edge effects do not seem to

strongly affect the debris population. These results match the phenomenology schematically depicted in Fig. 8, as well as previous experiments reported. Quantitative analysis, similar to that shown in Signor *et al.* (2010) for debris collected in PVC foams, is to be made with three-dimensional X-ray micro-tomography to extract volumetric distribution of fragments (size and number). High resolution is necessary to capture sub-micrometric fragments.

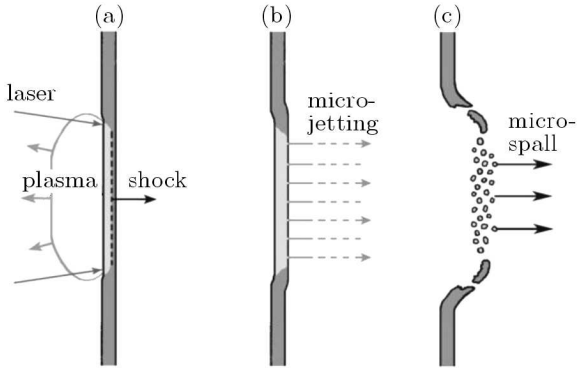

Fig. 8. Phenomenological interpretation of laser shock-induced 'micro-spall' in a 50 μm-thick tin sample. Melting is assumed to occur throughout the sample thickness, either on compression or on release

The 80 GPa laser shock on the 200 μm-thick aluminium target leads to a very different tableau (Fig. 9). Some partial melting occurs near the loaded surface, but due to shock pressure decay with propagation distance, most of the sample remains solid, so that spall fracture is the predominant fragmentation mechanism, with a spall strength of about 1.8 GPa (tension) in solid aluminium at the extreme strain rate involved here. It leads to ejection of solid spalled layers from the free surface (Fig. 9c). The fastest one is seen to fly at about 3.5 km/s, followed by a continuous debris cloud (Fig. 6), then it penetrates about 7 mm deep into the gel. This picture is consistent with one-dimensional computations of laser-matter interaction and shock propagation (Fig. 7). Further deformation of the target leads to full opening, explaining the final hole (Fig. 4), as well as ejection of both solid and liquid (coming from the vicinity of the irradiated surface) secondary fragments (Fig. 9d), which penetrate into the gel behind the main spall. To reach the microspall regime for such a thick aluminium foil, the shock pressure (i.e. laser intensity) should be increased, and/or sample should be preheated to lower the pressure required for shock-induced melting.

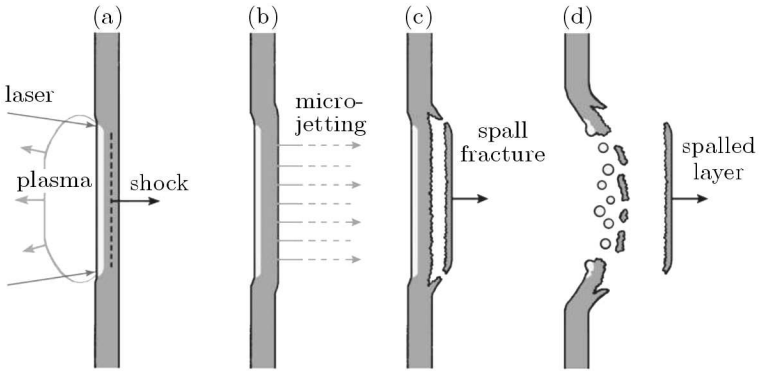

Fig. 9. Phenomenological interpretation of laser shock-induced fragmentation in a 200 μm-thick aluminium sample. Partial melting is assumed to occur only over a limited depth beneath the loaded surface (left), then shock pressure decays below the melting conditions, so that spall fracture takes place in the solid region

6. Conclusion

Dynamic failure and fragmentation of shock-loaded tin and aluminium have been investigated using a laser shock generator and complementary diagnostics methods (scanning electron microscopy, optical shadowgraphy, soft recovery technique involving a low density gel). The energies involved in laser shock experiments are lower than in conventional shock techniques, e.g. plate impact experiments, so they are less destructive. This allows one to carry out an original post mortem examination of targets and fragments. Analysing the recovered ejecta leads to evaluation of the number and of characteristic size spectrum of the fragments. As illustrated in this work and from earlier studies, the fragmentation in microspalled (liquid) tin involves micrometric and sub-micrometric particles. In regard to aluminium tested in loading conditions near melting on release, the fragments sizes are found to range from some $\sim 10\,\mu$m to some mm after a combination of spall fracture (solid state) and secondary fragmentation in partially melted regions near the loaded surface. It is shown that even in solid state, the fragmentation process is far more complex than the idealized succession of well defined spalled layers. Further work is needed to better understand the evolution of this process from spalling to microspalling in a variety of structural metals.

Acknowledgments

We thank all the staff of the LULI and the Alise team for technical support, as well as Pierre-Henri Maire, Jérôme Breil and Guy Schurtz for providing access to the code CHIC.

References

1. Andriot P., Chapron P., Lambert V., Olive F., 1984, Influence of melting on shocked free surface behaviour using Doppler laser interferometry and X-ray densitometry, *Proc. Shock Waves in Condensed Matter*, Asay J.R., Graham R.A., Straub G.K. (Eds.), North-Holland Amsterdam, 277-280
2. Antoun T., Seaman L., Curran D.L., Kanel G.I., Razorenov S.V., Utkin A.V., 2002, *Spall Fracture*, Springer, New York
3. Asay J.R., Mix L.P., Perry F.C., 1976, Ejection of material from shocked surfaces, *Applied Physics Letters*, **29**, 5, 284-287
4. Barker L.M., Hollenbach R.E., 1972, Laser interferometer for measuring high velocities of any reflecting surface, *Journal of Applied Physics*, **43**, 4669-4675
5. Bushmann A.V., Lomonosov I.V., Fortov V.E., 1992, Equation of state for metals at high energy density, *Technical report of Institute of Chemical Physics*, Chernogolovka
6. De Resseguier T., Signor L., Dragon A., Boustie M., Roy G., Llorca F., 2007a, Experimental investigation of liquid spall in laser shock-loaded tin, *Journal of Applied Physics*, **101**, 1, 013506
7. De Resseguier T., Signor L., Dragon A., Severin P., Boustie M., 2007b, Spallation in laser shock-loaded tin below and just above melting on release, *Journal of Applied Physics*, **102**, 7, 073535
8. De Resseguier T., Signor L., Dragon A., Boustie M., Berthe L., 2008, On the dynamic fragmentation of laser shock-melted tin, *Applied Physics Letters*, **92**, 13, 131910
9. De Resseguier T., Signor L., Dragon A., Roy G., 2010, Dynamic fragmentation of laser shock-melted tin: experiment and modelling, *International Journal of Fracture*, **163**, 1/2, 109-119
10. Elias P., Chapron P., Laurent B., 1988, Detection of melting in release for a shock-loaded tin sample using the reflectivity measurement method, *Optics Communications*, **66**, 2/3, 100-106
11. Eliezer S., Gilath I., Bar-Noy T., 1990, Laser-induced spall in metals: experiment and simulation, *Journal of Applied Physics*, **67**, 715-724
12. Grady D.E., 1988, The spall strength of condensed matter, *Journal of the Mechanics and Physics of Solids*, **36**, 3, 353-384
13. Grady D.E., 1996, Spall and fragmentation in high-temperature metals, high-pressure shock compression of solids, In: *High-Pressure Shock Compression of Solids. II Dynamic Fracture and Fragmentation*, Davison L., Grady D.E., Shahinpoor M. (Eds.), Springer, New York Ch.9, 219-236

14. Henis Z., Eliezer S., 1993, Melting phenomenon in laser-induced shock waves, *Physical Review E*, **48**, 3, 2094-2097

15. Klepaczko J.R., Chevrier P., 2003, A meso-model of spalling with thermal coupling for hard metallic materials, *Engineering Fracture Mechanics*, **70**, 2543-2558

16. Lescoute E., de Resseguier T., Chevalier J.M., Boustie M., Cuq-Lelandais J.P., Berthe L., 2009, Soft recovery technique to investigate dynamic fragmentation of laser shock-loaded metals, *Applied Physics Letters*, **95**, 211905

17. Mercier P., Benier J.,Frugier P.A., Sollier A., Rabec Le Gloahec M., Lescoute E., Cuq-Lelandais J.P., Boustie M., de Resseguier T., Claverie A., Gay E., Berthe L., Nivard M., 2009, PDV Measurements of NS and FS Laser driven shock experiments on solid targets, *Proc. Shock Compression of Condensed Matter*, American Institute of Physics, **1195**, 581-584

18. Nowacki W.K., 1978, *Stress Waves in Non-Elastic Solids*, Pergamon, Oxford

19. Signor L., de Resseguier T., Rot G., Dragon A., Llorca F., 2007, Fragment-size prediction during dynamic fragmentation of shock-melted tin: recovery experiments and modelling issues, *Proc. Shock Compression of Condensed Matter*, American Institute of Physics, **955**, 593-596

20. Signor L., Dragon A., Roy G., de Resseguier T., Llorca F., 2008, Dynamic fragmentation of melted metals upon intense shock wave loading. Some modelling issues applied to a tin target, *Archives of Mechanics*, **60**, 4, 323-343

21. Signor L., de Resseguier T., Dragon A., Roy G., Fanget A., Faessel M., 2010, Investigation of fragments size resulting from dynamic fragmentation in melted state of laser shock-loaded tin, *International Journal of Impact Engineering*, **37**, 8, 887-900

22. Tollier L., Fabbro R., 1998, Study of the laser-driven spallation process by VISAR interferometry technique. II. Experiment and simulation of the spallation process, *Journal of Applied Physics*, **83**, 3, 1231-1237

Dynamiczna defragmentacja metalu topionego impulsem laserowym: wybrane rezultaty badań doświadczalnych

Streszczenie

O ile problem łuszczenia i wykruszania się materiałów pod wpływem obciążeń udarowych został bardzo szeroko przeanalizowany, bardzo niewiele informacji spotyka się odnośnie odpryskiwania metali w stanie płynnym. Niektórzy z autorów obecnej

pracy przeprowadzili badania nad odpryskiem płynnym, czasem zwanego mikroodpryskiem, polegającym na dezintegracji materiału stopionego impulsami laserowymi o dużej mocy. Zaproponowali oni także sposób modelowania tego zjawiska, weryfikując go z wynikami eksperymentalnymi. W szczególności, rozkłady teoretyczne rozmiaru odprysku porównano z wynikami doświadczeń, gdzie metodami analizy obrazu zmierzono rozmiar odpryśniętych cząstek uwięzionych w specjalnych ekranach polimerowych umieszczonych za próbką. Zauważono, że analityczne krzywe rozkładu reprezentujące liczbę odłamków na jednostkę powierzchni w funkcji wielkości tych odłamków pozostają w zgodzie z eksperymentem, jednak już sama ilość zdefragmentowanego materiału wynikającego z modelu energetycznego znacznie przewyższa rezultat doświadczalny. Ta nadwyżka wynika głównie ze stosowanej metody zliczania ilości odprysku, ograniczającej się jedynie do badań powierzchniowych, tymczasem część odprysku penetruje ekran polimerowy znacznie głębiej. Z tego powodu w niniejszej pracy zaproponowano i przetestowano nową metodę jakościowego i ilościowego określania odprysku oraz przedyskutowano jej skuteczność. Nowa metoda bazuje na zastosowaniu zamiast ekranów polimerowych przezroczystego żelu o małej gęstości, umożliwiającego łatwą obserwację (w porównaniu do pianek i aerożeli) wielkości odpryskiwanych cząstek, ich kształtu oraz głębokości penetracji przy zwiększonej rozdzielczości przestrzennej obrazu. Technika ta, wspomagana cieniografią oraz mikrografią optyczną i elektronową (mikroskop skaningowy), stanowi zaawansowane narzędzie do badań nad zjawiskiem mikroodprysku. Do prezentacji skuteczności tej metody przeprowadzono doświadczenia nad próbkami z cyny i aluminium przy różnych warunkach topienia i defragmentacji pod wpływem impulsu laserowego.

Manuscript received April 15, 2010; accepted for print June 7, 2010